Visualization and Analysis of Rotating Stall for Transonic Jet Engine Simulation

Chun-Ming Chen, Soumya Dutta, Xiaotong Liu, Gregory Heinlein, Han-Wei Shen, *Member, IEEE*, and Jen-Ping Chen

Abstract— Identification of early signs of rotating stall is essential for the study of turbine engine stability. With recent advancements of high performance computing, high-resolution unsteady flow fields allow in depth exploration of rotating stall and its possible causes. Performing stall analysis, however, involves significant effort to process large amounts of simulation data, especially when investigating abnormalities across many time steps. In order to assist scientists during the exploration process, we present a visual analytics framework to identify suspected spatiotemporal regions through a comparative visualization so that scientists are able to focus on relevant data in more detail. To achieve this, we propose efficient stall analysis algorithms derived from domain knowledge and convey the analysis results through juxtaposed interactive plots. Using our integrated visualization system, scientists can visually investigate the detected regions for potential stall initiation and further explore these regions to enhance the understanding of this phenomenon. Positive feedback from scientists demonstrate the efficacy of our system in analyzing rotating stall.

Index Terms—Turbine flow visualization, vortex extraction, anomaly detection, juxtaposition, brushing and linking, time series

1 Introduction

The study of turbine engine stability has been an ongoing research in aerospace engineering. In spite of the advances in technologies, the optimum performance of jet engines is still limited by the safe operation of the compressors. This limitation is mainly due to the emergence of the *rotating stall* when the operating range is pushed beyond the safety limit. The rotating stall is a local disturbance in the airflow through the turbine blades, which propagates among blade passages in the opposite direction of the rotor, thus increasing the loading of the blades. Although subtle initially, sustained rotating stall can eventually lead to violent system instability causing destructive damage to the engine. Therefore, early detection of stall inception is essential to obtain sufficient response time in order to prevent engine failure.

Due to the recent advancements of parallel computing capabilities, application scientists can now perform high accuracy numerical simulations based on computational fluid dynamics (CFD) techniques in high resolutions. The results of the simulations contain rich information aiding domain scientists in understanding the complex nature of rotating stall. More specifically, researchers want to investigate: (1) the early signs of the rotating stall and (2) which local regions show such signs and at what time step? The identification of early signs of stall in the simulation data is important because the scientists can then study the simulation data around the detected time step in order to develop new stall precursors for practical use. However, since the size and complexity of the simulated unsteady data become significantly large, it poses unique challenges for the domain scientists to efficiently process or explore the simulation results in order to understand the stall phenomena. Moreover, stall analysis involves temporal data analysis, which requires appropriate visualization techniques that can effectively convey the extracted information from the time-varying data. The domain scientists also need to visually verify the occurrence of stall once it is detected through the hypothesized stall precursor analysis methods. Therefore, it is required to provide a visual analytics system that includes the domain scientists in the exploration loop, where they can synthesize and verify hypotheses through visualized interaction with the data.

In this paper, we present a workflow for the analysis and visualization of transonic jet engine simulation data undergoing rotating stall. We first utilize existing stall precursor techniques to identify time steps and blade passages which are more susceptible to stall. Based on a recent study in turbomachinery, stall can be identified by tracking the trajectories of vortices close to the blade tips over time [23]. We provide an efficient algorithm to extract and analyze the vortices from the simulation data. Furthermore, since rotating stall initiating in local regions of the rotor can be characterized as local disturbances, we introduce a novel method of instability analysis by detecting statistically anomalous regions among the blade passages. To effectively convey the analysis results over all blade passages and time steps, visual comparison tools using interactive juxtaposed plots are devised to reveal patterns allowing the scientists to quickly identify time periods and blade passages undergoing potential rotating stall. Once an interesting temporal and spatial region is located, a unified visualization system incorporating several spatial data visualization techniques allows the user to visually verify the suspected regions and further explore the data. Feedback from the domain scientists shows that the proposed integrated visual analytics system can substantially reduce the search space of the problem. Also, the patterns revealed by the proposed visualization methods for the stall analysis results demonstrate the potential for earlier identification of stall inception. Therefore, the contributions of this work to stall analysis and visualization are threefold:

1. Efficient algorithms for detecting stall precursors using an existing vortex analysis technique and a new statistics based method are proposed. The later is shown to be able to detect stall early in our study.
2. Comparative visualization techniques are applied to the above analysis results to facilitate visual identification of abnormalities that lead to stall.
3. A visual analytics framework for stall study is presented that integrates temporal and spatial visualization techniques for stall detection, verification, and further exploration in large datasets.

The structure of the rest of this paper is as follows: Section 2 discusses the related works and techniques. In section 3 we provide further information about stall and its known precursors. Section 4 presents our stall precursor analysis method, followed by our visual exploration framework for the verification of the precursors in Section 5. The results are shown in Section 6, and discussed in Section 7. We conclude the paper in Section 8.

- *Chun-Ming Chen, Soumya Dutta, Xiaotong Liu and Han-Wei Shen are with The Department of Computer Science and Engineering, The Ohio State University. E-mail: {chen.1701, dutta.33, liu.1952, shen.94}@osu.edu.*
- *Gregory Heinlein and Jen-Ping Chen are with The Department of Mechanical and Aerospace Engineering, The Ohio State University. E-mail: {heinlein.29, chen.1210}@osu.edu.*

Manuscript received 31 Mar. 2015; accepted 1 Aug. 2015; date of publication 20 Aug. 2015; date of current version 25 Oct. 2015.
For information on obtaining reprints of this article, please send e-mail to: tvcg@computer.org.
Digital Object Identifier no. 10.1109/TVCG.2015.2467952

2 Related Work

To the best of our knowledge, this work is among the first visual analytics frameworks specific for the study of turbine engine stall. In a broader scope, visual analysis of different types of turbine flow has been studied in various purposes. Sadlo *et al.* [38] proposed a framework for design optimization of a hydraulic turbine, which focused on visualization of vorticies and analysis of vorticity distribution. In the analysis of power output in wind turbines, Shafii *et al.* [43] proposed a framework to analyze vortex-turbine interaction. Downstream vortices are visualized in vortex hulls and the degrees of intersection are color coded on the turbine blades, along with plots of related measures over time. Among works submitted to IEEE Visualization Contest 2011 on the study of a centrifugal pump turbine, Yee *et al.* [8] argued that detailed variations are easily missed in video presentation. To summarize vortices detected from all time series, they proposed a single-image summarization technique that visualizes vortices in ribbons.

Compared to previous research on related problems, our work focuses on the identification of abnormalities and patterns from large-scale time series data. As scientists are still exploring the criteria to detect stall inception, the current approach is through comparing flow phenomena in different blade passages and time steps. Therefore, in our problem comparative visualization of different time steps is more important than rendering the solution of a single time step. To analyze large unsteady data and provide effective summary visualization of all passages and time steps, techniques including efficient vortex detection, anomaly analysis, as well as brushing and linking are used.

Vortex analysis in our work as well as all the above turbine-related works is an important means to understand the underlying flow phenomena. Jiang *et al.* [26] provided a review of different types of vortex detection methods. Depending on the choice of vortex definition, they categorized vortex detection methods into line based and region based approaches. Line based approaches detect and connect points of vortex cores to generate *vortex core lines*; region based approaches instead detect possible points associated in vortex regions. In general, line based approaches provide compact representation of vortices but region based approaches are computationally cheaper.

In our approach, λ_2-criterion [25] is used to efficiently extract vortex regions. λ_2-criterion for vortex detection has been applied in many previous studies for flow analysis purposes [29, 41, 44], as well as in the aforementioned works of turbine analysis. The method evaluates the Jocobian of flow velocities surrounding a given point, and label the point based on the eigenvalues of the matrix $[S^2 + R^2]$, where S is the rate-of-strain tensor and R is the rate-of-rotation tensor. The points that get negative second-largest eigenvalues (a.k.a. λ_2) are considered as part of a vortex region, and the more negative the value the more probable it is in a vortex. Alternative region based vortex measure Q-criterion [24] has also been widely used.

Anomaly or outlier detection has been studied in a variety of fields including statistics, machine learning and data mining with different data models and anomaly types [2, 9, 22]. In statistics, outliers are determined according to a presumed distribution, typically a normal distribution. Z-test detects outliers by examining each sample value and computing its deviation from the mean. If any of these deviations is larger than a scalar multiple, typically 1.96x, of the standard deviation, the corresponding sample is considered as an outlier. Since the underlying standard deviation of the data is typically unknown, and using the standard deviation computed from the small number of test samples can be biased from outliers, Grubbs' test [20] is thus advantageous in determining the proper scalar multiple according to the number of samples. More advanced statistics approaches to obtain model parameters in time series include regression based methods [1] and EM algorithms [16]. In this work we use Grubbs' test for anomaly detection among the blade passages to detect the sign of instability.

Besides statistics approaches, when the data distribution is unknown, distance based methods like k-nearest neighbors are generally used, with time complexity typically higher than linear complexity [28, 35]. Alternatively, when a subset of data can be labeled to be normal or abnormal, supervised approaches are used to train the data model for anomaly detection [18].

Juxtaposition (or small multiples [5, 46]) is an effective visual design that encourages side-by-side visual comparison of multiple facets of a complex data set, without overplotting or occlusion that may occur in shared space techniques [17]. This comparative visualization has been used in many applications such as parameter space analysis, stock market trend analysis, census demographics, climatology and network analysis for various visualization plots such as bar charts, line charts, and adjacency matrices [27, 30, 31, 47].

Brushing and linking are interaction techniques commonly used to enhance scatterplot matrices [4, 6], parallel coordinates [3, 15] and other small multiple views [37]. The user brushes with an input device on one plot and the linked data points on other plots are highlighted concurrently. This effectively associates plots from different views of the data together. In combining scientific and information visualization views, Gresh *et al.* [19] proposed WEAVE, which allows users to brush on 2D statistics and 3D spatial views of data. Doleisch [14] introduced SimVis, which integrates several visualization techniques including smooth brushing with fuzzy classification and time-dependent feature specification for unsteady CFD data. In our work, we extend the user interaction of brushing and linking to the search of the first occurrence of a qualified event, i.e. possible stall inception among the juxtaposed scatter plots of the temporal data.

3 Motivation, Background and Approach Overview

Stall inception has been actively researched for the past few decades. Although modern engine manufacturers can estimate the engine's safe operating range and impose a safety margin for unpredictable manufacturing variances, scientists and engineers still strive for narrowing the margin to obtain increased engine performance by suppressing any instability once it is detected. Therefore, to obtain sufficient response time before engine failure, early detection of stall is an important research to the related fields. Among instances of engine failure, rotating stalls have been identified as a cause of destructive flows. A rotating stall starts from localized flow separation from a turbine blade surface, which disrupts normal path of flow and forms small *stall cells* in the blade passages. Instead of following the bulk airflow direction, the stall cells propagate around the rotor at a slower rotating speed than the blades, thus inducing unbalanced forces on the turbine blades. The initial signs of stall cells can be subtle and intermittent, but sustained stall cells can quickly grow and become destructive to a compressor. To identify stall cells, it is required to observe the evolution of abnormal flow behaviors over time instead of at a single instance, thereby increasing the complexity of analyzing rotating stall. Traditionally, measures such as mass flow rate and pressure probe-based analysis have been widely adopted to detect rotating stall. However, these methods still have their limitations at predicting when stall will occur, which will be described in Section 3.1.

With the advances of computation performance on supercomputers in the past decade, analyzing data generated from numerical simulations opens new opportunities for stall precursor research. A high-resolution CFD solver, TURBO [10], has recently been proven to be capable of capturing the major characteristics of stall [11]. However, the large size of the simulation results and the lack of visualization tools specific to the problem pose significant challenges for the scientists to study the data. Therefore, in this work, we present an analysis and visualization framework which extracts pertinent information for stall analysis from large scale simulation data.

The datasets used in our experiments are generated from simulations of a NASA single-stage compressor [36], which is a representative model of transonic axial compressor. The geometry of the rotor consists of 36 blade passages, shown in Figure 1. The solutions are computed by TURBO, which solves the Navier-Stokes equations in the full-annulus model. TURBO generates high-resolution unsteady flow fields for all passages, which are then analyzed in our framework to enhance the understanding of rotating stall. Several simulations were performed with different operating conditions that will lead to stable or stall conditions for the purpose of studying the transitions between them. In the following we first use a simulation dataset of a stall condition to explain and formulate our stall detection and analy-

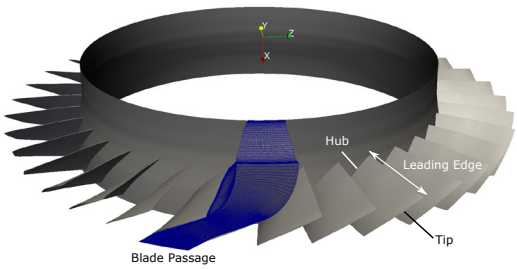

Fig. 1: The compressor rotor in our dataset with highlighted terminologies.

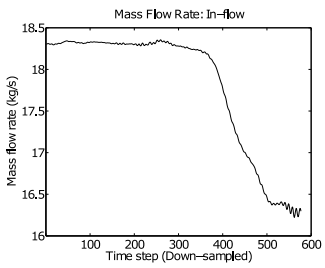

(a) Mass flow rate plot. The rapid drop indicates the occurrence of stall.

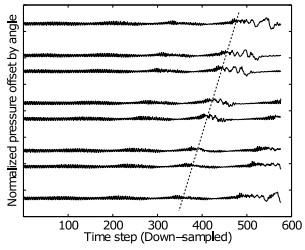

(b) Pressure probe plot. The dotted line indicates the propagation of disturbance across different probes.

Fig. 2: Traditional stall detection methods and the plots.

sis method. In the result section, other conditions are tested to verify and demonstrate the effectiveness of our method. Below we provide an overview of the existing stall analysis techniques and then describe the motivations behind the choices of precursors in this work.

3.1 Traditional Stall Detection Methods

In this section, we discuss two typical techniques for analyzing stall in engines along with their limitations.

Mass flow rate is a standard measure to verify the existence of stall in numerical experiments [21, 32, 48], which reflects the mass of air that flows through the compressor per unit time. The mass flow rate, denoted by $\dot{m}$, is defined as:

$$\dot{m} = \rho \mathbf{v} \cdot \mathbf{A}, \tag{1}$$

where ρ represents the density and $\mathbf{v}$ is the flow velocity. $\mathbf{A}$ is the area vector of a surface, which is the cross section of the inlet or exit of the compressor stage for stall analysis. It has been shown that when a system undergoes a rotating stall, the mass flow rate drops significantly. A plot of mass flow rate against time in Figure 2a shows a characteristic curve of the mass flow rate drop under stall conditions. It can be observed that from around time step 250 onwards the mass flow rate starts to decrease, and it drops rapidly after around time step 350. By observing the drop of the mass flow rate, scientists can explicitly identify the occurrence of stall. Although the mass flow rate plot is commonly used in stall analysis, it does not serve as a stall precursor because mass flow rate drops after stall occurs. Moreover, since mass flow rate is a global measure, it does not provide detailed phenomena or specific regions of stall in data for further analysis.

Use of **pressure probes** in stall detection has been extensively studied and adopted widely in practice [12, 13, 33]. The probes are located circumferentially within the engine casing to record the pressure oscillation over time. Since the pressure in stall cells is distinct from that of their surrounding areas, pressure probes can capture these spikes in value once a stall cell passes a probe location. Figure 2b shows the pressure probe plot used by the scientists to analyze stall. In the figure, eight curves represent eight pressure probes in different angular locations, where each curve is a plot of the pressure values over time. It can be seen that the oscillation of each curve changes drastically when stall occurs after time step 350 and the abnormality shifts to the next probe as the stall cells rotate. By correlating the occurrence of stall cells detected by pressure probes located at different circumferential locations, the scientists can estimate their rotation speed. When this speed drops close to half of the rotor speed, stall will occur imminently. In spite of numerous successful stall analysis approaches based on pressure probing, it is nontrivial to find the proper probe locations and the number of probes to use, which can be different for different compressor models. Moreover, the current pressure probe plotting can only convey a few probes per chart. When the number of curves representing the pressure probes increases, the chart becomes cluttered and difficult to visually identify oscillation changes.

3.2 Problem Statement

High resolution data generated from CFD simulations provide rich information that allows scientists to conduct detailed studies of engine stall. However, it also poses significant challenges to analyze the large amount of data that are produced. Since stall analysis requires observing the temporal evolution of flow behaviors, our goal is to help the domain scientists visually detect early stall inception from its temporal patterns and verify the detected regions with their domain knowledge. With a well-designed visual analytics framework to help identify time steps and regions of possible stall inception, the exploration time and effort for stall analysis can be substantially reduced.

The visual analytics system will meet the following requirements set by the scientists:

1. Analyze the dataset based on selected stall detection methods.
2. Visualize the stall analysis results with sufficient information for the scientists to identify salient time steps and regions for possible stall inception.
3. Once an important spatiotemporal region is selected, render the corresponding data for visual verification of the phenomena and allow a more detailed exploration of the region.

Next we provide an overview of our visual-analytic framework.

3.3 Overview of The Visual Analytics Workflow

Figure 3 presents a schematic view of the stall analysis and exploration framework. The proposed framework processes large scale unsteady data and extracts information using two stall analysis methods based on domain knowledge. The first method uses a stall precursor proposed by Hoying *et al.* [23], which detects stall based on the orientation of the tip clearance vortex in each blade passage. We automate the detection using vortex extraction techniques on the velocity fields and calculate the orientation of each vortex structure. In the second method, inspired by the use of pressure probes to detect abnormal value changes, we adopt a statistical method to detect anomalies among the blade passages. These analysis methods measure the tendency of stall inception for all time steps of data in the preprocessing stage, which will be described in Section 4.

Once the related information to stall analysis is extracted, the results are presented in interactive visualizations revealing the temporal trends. By observing the temporal and spatial patterns in the visualization, the scientists are able to determine time steps and blade passages of possible stall inception for further analysis. After a salient spatiotemporal region is identified, the system then allows the scientists to explore the raw data at the specific time step in customized visualization, where they can verify the hypothesis of stall inception and explore the dataset to design new precursors. The visual comparison and exploration framework will be described in Section 5.

4 Detailed Descriptions of Stall Analysis Methods

Although the detection of stall has been under research for several decades, the actual phenomena that cause the inception of stall are still not completely understood. There is a growing need of novel stall precursors which can detect early signs of rotating stall with sufficient accuracy. In this section, we describe our techniques to compute the tip clearance vortex angles for stall detection and provide a statistical analysis method for finding anomalies in the data. Since the dataset is

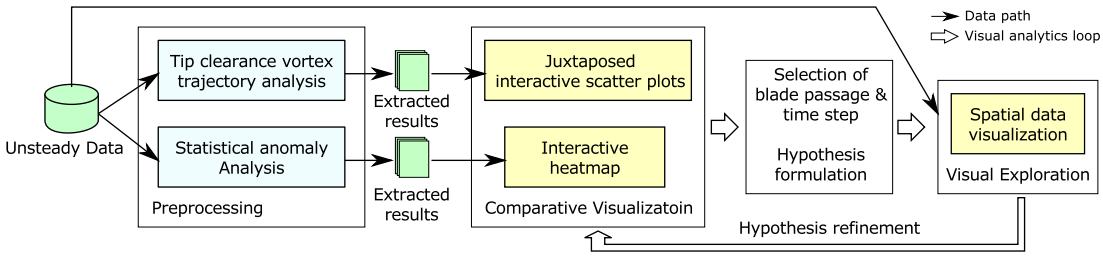

Fig. 3: Overview of the visual analytics framework.

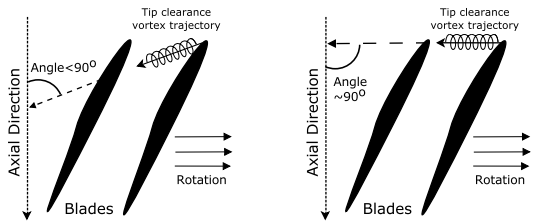

(a) Tip vortex in a healthy condition. (b) Tip vortex in a stall condition.

Fig. 4: A stall precursor based on the trajectory of the tip clearance vortex. Here the side view of the rotor is shown. The major flow direction follows the axial direction.

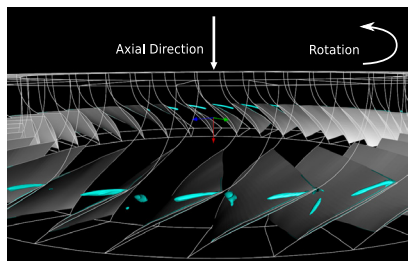

Fig. 5: Vortices found by the λ_2 criterion. The largest vortex close to the blade tip in each passage is the tip clearance vortex.

large in size, the analysis procedure should be efficient and only scan the data once. Accordingly, the stall analysis methods are designed with a minimum number of parameters, which extract sufficient but compact information to allow the user to adjust parameters in the interactive visualization. The extracted information will help the scientists efficiently identify time steps and blade passages of stall inception.

4.1 Stall Analysis Using Tip Clearance Vortex Trajectory

According to previous research, a well structured vortex, called a tip clearance vortex, usually forms on a blade tip under stable operating conditions. Normally these vortices do not inhibit flow through the blade passages. However, as the compressor nears a rotating stall, the tip clearance vortices start to move in a specific direction and eventually breaking down. Hoying *et al.* [23] hypothesized that when the angle of the tip clearance vortex core becomes perpendicular to the axial direction, the condition is approaching stall. A conceptual diagram depicting this phenomenon is presented in Figure 4. Figure 4a shows the state of tip clearance vortex in a healthy condition; Figure 4b presents the idea of a near stall condition when the angle between tip clearance vortex and axial direction is close to 90°. Hence, by observing the trend of the change of these angles, potential blade passages which show early signals of a rotating stall can be identified.

Although stall can be detected through analyzing the tip clearance vortices, automatic extraction and tracking of these vortices is not trivial. Since the location and orientation of the tip clearance vortex can vary from blade to blade, it is difficult to identify the tip clearance vortex from the other vortices in a blade passage automatically. We use prior knowledge from the scientists that the tip clearance vortex can be seen close to the blade tip in a passage and is usually the largest. Therefore the search area of vortices can be reduced to one third of the entire passage region toward the tip as the *target search region*. For each detected vortex we measure and store the length and the angle made with the axial direction, which is described as follows.

In order to efficiently detect vortices from all passages and time steps, region based vortex detection method λ_2-criterion [25] is used. As introduced in Section 2, negative λ_2 measures indicate the corresponding point is in a vortex region, with the more negative the value the higher possibility it is in a vortex. We allow the domain expert to examine and tune the threshold by rendering the extracted vortices from selected time steps in the user interface. This chosen threshold value is then fixed for vortex extraction processes during the remainder of the experiments. Since the tip clearance vortex is generally larger than other vortices in the same passage in normal conditions and even in near-stall conditions, we use a higher (more negative) threshold to filter out small or ill-structured vortices. This allows us to compute its angle to the axial direction with less noise, before it breaks down at stall. Figure 5 shows a sample isosurface rendering on λ_2 criterion where the structures of the tip clearance vortices are visible.

Since there may still exist several vortices in the search region, before measuring the orientation of each vortex region, we employ a connected component labeling algorithm [49] to label the detected points based on their spatial connectivity, where two neighboring points in the grids are considered connected. The algorithm scans through each point and labels the points by a group ID, where connected points are given the same ID. By doing so, points in different vortices are grouped separately, from which the respective lengths of the vortex cores and their angles to the axial direction can be extracted.

Since the tip clearance vortices are usually straight as shown in Figure 5, the principal component analysis (PCA) is used to extract the principal direction of each connected point group. From the result of PCA, we select the direction of the principal eigenvector $\vec{v}$ as the direction of the current vortex core and measure its angle Θ with axial direction $\vec{A_{dir}}$. The vortex length is approximated by two times the principal eigenvalue.

The presented algorithm is efficient because both the λ_2 criterion and the connected component labeling only require point-wise scans through the data points. In order to identify stall inception with higher confidence, the scientists would like to see the increasing trend of the tip clearance vortices to be perpendicular to the axial direction. Therefore we store the computed lengths and angles of vortices detected in each blade passage. Combined with our overview visualization showing the temporal changes of vortex angles in all the blade passages, the expert can more easily detect early signs of rotating stall, which will be described in Section 5.1.1.

4.2 Statistical Anomaly Detection for Rotating Stall Analysis

While the tip clearance vortex analysis provides one aspect of stall detection, we devise a statistics-based anomaly detection method to reveal more information from the simulation results. This method is inspired by how stall is commonly analyzed and detected from pressure probe readings, through observing irregularity of the pressure values. In a healthy condition, it is expected that the recorded pressure values

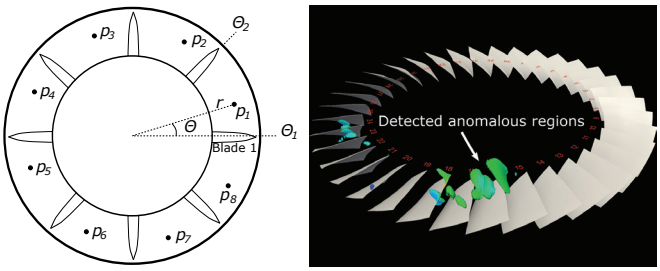

(a) (b)

Fig. 6: (a): Illustration of points extracted by the anomaly detection algorithm. All the points $p_1, ...p_8$ in the eight passages of this simplified example have the same radius r and relative angle θ. (b): Anomalous regions of pressure detected in a time step.

by each probe exhibit periodicity every time a blade passage passes a probe location. This is because the blades are axisymmetrically similar, so ideally the flow behaviors among the blade passages should also be axisymmetric. When stall cells appear within the passages, this symmetry breaks down and thus pressure probes are able to detect the stall cells since abnormal pressure oscillations are observed in the readings. Therefore, we extract sets of axisymmetric points from the passages and detect point-wise anomalies for each point set.

In order to efficiently detect point-wise anomalies from large unlabeled datasets, we adopt Grubbs' outlier test [20] for each point set in symmetry, assuming these points form a normal distribution in a normal condition. Grubbs' test is widely used for its computational simplicity [45]. It is more robust than the simpler Z-test when the standard deviation of the data distribution is unknown, as mentioned in Section 2. Note that Grubbs' test is not applicable if too many outliers exist in the sampled data. However, since our goal is to detect early signs of stall inception, it can be expected that outliers are less observed in relatively normal conditions.

To detect anomalies in the flow field, for each time step we first group points from each passage that are at the same relative position into a point set. The number of point sets is equivalent to the number of grid points in a passage. Figure 6a illustrates a simplified rotor to facilitate understanding, in which one point from each passage has the same relative position and will therefore be grouped together.

Formally, in a compressor of m blade passages, a point in the k-th blade passage, $1 \leq k \leq m$, can be defined as

$$p_k(x,r,\theta) = \langle x, r, \theta + \theta_k \rangle \tag{2}$$

in the cylindrical coordinate, where r is the radius from the center and θ is the relative angular offset from the referencing angle θ_k of the k-th passage. x represents the axial position toward turbine downflow, which is the direction pointing into the paper.

For each set of points $p_1 \cdots p_m$ at the same relative position in each passage, we form a value set $\mathbf{V}$:

$$\mathbf{V} = \{f(p_k(x,r,\theta))|k = \{1,2,...,m\}\} \tag{3}$$

where $f(p)$ is the field value (pressure) at point p. Then for each point set we apply Grubbs' test by first computing the mean $\mu(\mathbf{V})$ and standard deviation $\sigma(\mathbf{V})$ of these values. Based on Grubbs' test, a value $\mathbf{V}_k$ is an outlier of set $\mathbf{V}$ if

$$\frac{|\mathbf{V}_k - \mu(\mathbf{V})|}{\sigma(\mathbf{V})} > \frac{m-1}{\sqrt{m}} \sqrt{\frac{t^2_{\alpha/(2m),m-2}}{m-2+t^2_{\alpha/(2m),m-2}}}. \tag{4}$$

Here $t_{a,v}$ is the critical value of the t-distribution with the alpha value $a = \alpha/(2m)$ and degrees of freedom $v = m-2$. For our case of anomaly detection, the significance level $\alpha = 0.01$ is used. Thus with the sample size $m = 36$ from 36 blade passages, the right hand side of the above inequality is around 3.3296.

We repeat Grubbs' test for all point sets in the dataset and extract anomalous points in terms of pressure values. Figure 6b presents one instance of the rotor where detected anomalous regions based on the pressure values are highlighted. Although the anomaly detection is performed individually for each point set, in the experiments we observe contiguous detected abnormal points in local neighborhood, which form larger anomalous regions in some passages.

Before further experiments were conducted to confirm the validity of our hypotheses, we showed the detected anomalous regions in selected time steps and the expert agreed that our approach has potential to capture the development of stall cells. However, since a detected anomalous region alone does not provide much evidence, the expert asked to see the temporal behavior of the anomalous regions for further verification. Therefore, we devised a compact visualization of detected anomalies from all time steps. From patterns revealed in the visualization, the expert confirmed that the detected regions are related to stall cells, as will be discussed in Section 5.1.2.

5 Visual Analytics Interface Design for Stall Analysis

In this section we present how the visual analytics system integrates appropriate visualization techniques for the scientists to easily identify spatial and temporal patterns from the stall analysis results. Since both of the above stall analysis methods are hypothesized to identify stall, in order to verify the hypotheses the scientists rely on (1) inspecting trends of the detected results to see how they evolve over time and how long the detected events persist, and (2) studying the flow data surrounding the detected regions to observe the temporal trend of the related variables. To achieve this systematically, in Section 5.1 we first introduce our comparative visualization interface that presents the trends of the precursor results through multiple juxtaposed charts. Once an important region is identified through the visualization, our visual exploration system allows verification and in-depth analysis of the detected results through spatial visualization techniques, as described in Section 5.2.

5.1 Comparative Visualization of Stall Analysis Results

In order to effectively help scientists identify potential stall inception in a large simulation dataset which stores thousands of time steps, we devise a comparative visualization tool to convey the results of stall precursor analyses over all time steps. Our comparative visualization tool satisfies the following design goals:

1. Can identify time steps and blade passages that are more susceptible to stall. This is done by comparing the measures of the stall analysis results.
2. Can reveal the temporal pattern of the analysis results. This is important because a single detected instance may not be significant enough to determine stall.
3. Can facilitate the detection of early signs of stall inception from the analysis results.

We describe the comparative visualization system for each of the stall analysis method separately in the following sections.

5.1.1 Comparative Visualization of Tip Vortex Angles

According to Hoying *et al.* [23], stall can be detected when tip clearance vortices become perpendicular to the axial direction. Although one can search for vortices around 90 degrees by a single scan of the vortex analysis result, visualization is necessary for the following two reasons: (1) Since a single instance may not be significant enough to determine stall, it is required to observe the increasing trend of the vortex angle toward 90 degrees over a longer time span. (2) With more information presented, the scientists are able to formulate new stall precursors with different criterion. Therefore, to effectively convey and compare the vortex analysis results for all time steps and all passages, we create an *interactive juxtaposed visualization* where the vortex angles for each passage are plotted against time and put side-by-side for contrast.

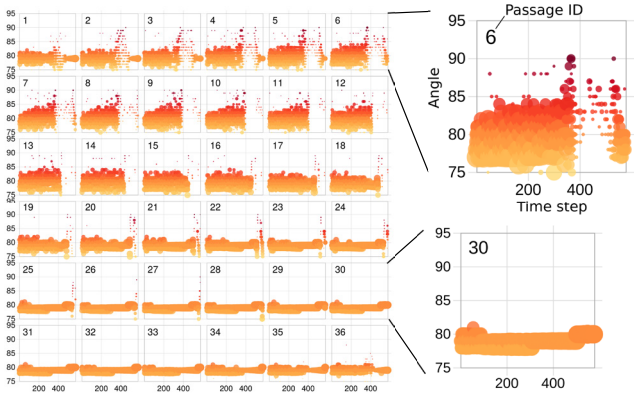

Fig. 7: The juxtaposed visualization of tip clearance vortex angles.

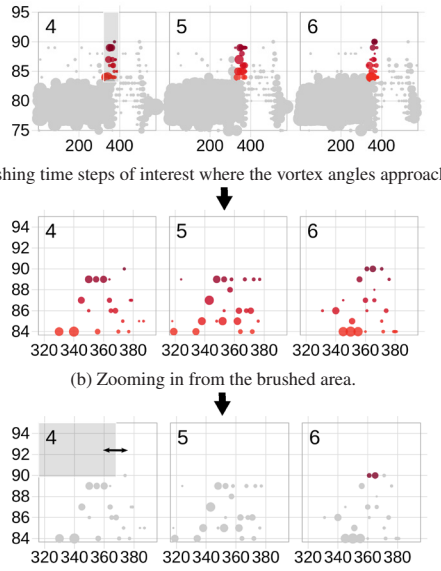

(a) Brushing time steps of interest where the vortex angles approach 90°.

(b) Zooming in from the brushed area.

(c) Highlighting angles around 90° in the earliest time steps. The size of the highlighted region can be easily adjusted to find the first qualifying instance among all passages.

Fig. 8: Illustration of the interface to find the first time step and passage where the tip clearance vortex first approaches 90°. Selected passages are shown for demonstration purpose. Please see the accompanying video for the demonstration.

To provide an overview of the tip clearance angles over all time steps and passages, it is desired that the visualization simultaneously presents attributes of each vortex including the angle, length and the ID of the passage it belongs to. Figure 7 shows the visualization of the vortex analysis result for the dataset in the stall condition previously presented in Section 3.1. In the juxtaposed visualization, each small chart corresponds to a blade passage where the horizontal axis represents time steps and the vertical axis represents vortex angle. Inside each chart, each extracted vortex is represented as a dot whose size is proportional to the corresponding vortex length and the color is modulated by the closeness of the angle to 90 degrees. If the color is close to dark red, the vortex is approaching 90 degrees.

Figure 7 shows an increasing trend of vortex angles toward 90 degrees, which is more easily seen in passages 2 to 13. Around time step 400, these passages show small and sparse dots, indicating the vortices break down. Concurrently, in passages 25 to 35 more stable and longer vortices (larger circles) are displayed with angles around 80 degrees.

To further investigate the time steps and passages where the vortex angles first approach 90 degrees, the interaction tool allows the user to brush (Figure 8a) and zoom into the angles and time steps of interest (Figure 8b). To look for the vortex that first becomes 90 degrees, the

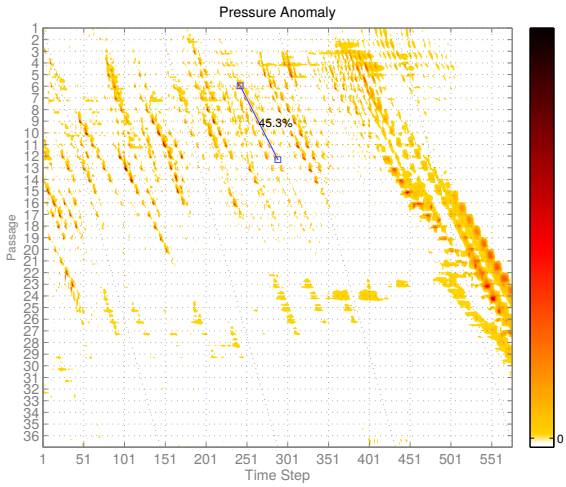

Fig. 9: Anomaly analysis chart of pressure values.

user can first select an area including degree 90 and then adjust the width of this area to change the selected time interval. As the user expands the area width, dots falling within the selected time and angle interval will be highlighted in all passages (Figure 8c). In this way, it is easy to contrast vortex angles and time steps across all passages and find the first occurrence of vortex within the desired angle range, which can be chosen other than 90 degrees to further explore the characteristics of the tip clearance vortices.

Figure 8c shows the highlighted dots representing the vortex angles first near 90 degrees, which starts from time step 361 in passage 6. This time step coincides with the rapid decrease of the mass flow rate shown in Figure 2a, but the tip clearance vortex analysis method provides a more specific time and location for investigating stall phenomena. The user can then select this passage and time step in the visual exploration tool for verification and further investigation, which will be described in Section 5.2.

5.1.2 Comparative Visualization of Statistical Anomaly

As discussed in Section 4.2, the anomaly detection algorithm attempts to identify abnormal regions, which can be stall cells that eventually cause a rotating stall. To verify this, it is required to see how these regions evolve over time. In general, the behavior of the anomalous regions can be classified into three broad types: (1) sporadically appearing and dissipating over a short time period, (2) remaining at a similar physical position over certain time steps, (3) moving along with the blades over certain time steps. In the study of stall inception, the scientists are more interested in detecting types (2) and (3) where the anomalous regions persist over a longer time span. Once they are detected, it is necessary to know the rotation speed of these hypothesized stall cells among passages.

To meet the above requirements, we utilize a 2D heatmap that encapsulates both the spatial and temporal patterns of the detected anomalous regions, as shown in Figure 9. Since we are more interested in how the anomalous regions move across passages over time and less in their movement within a passage, in the plot, the horizontal axis represents the time step and the vertical axis represents the angular position labeled by the passage ID. We use a colormap for the count of anomalous points detected in different radii(r) and axial positions(x) but in the same angular position, with darker color for a larger count.

Through the inspection of Figure 9, two major trends in the propagation of anomalous regions can be observed: (1) Horizontal direction, meaning the detected anomalies stay in the same blade passages, i.e., rotate at the same speed as the rotor over time; (2) slant direction, meaning these regions move across the blade passages, or rotate at a different speed than the rotor speed. It can also be seen that before time step 350, the chart shows fragmented but aligned slant patterns, as highlighted by the blue line. This means the anomalous region intermittently moves across passages, which pattern cannot be easily cap-

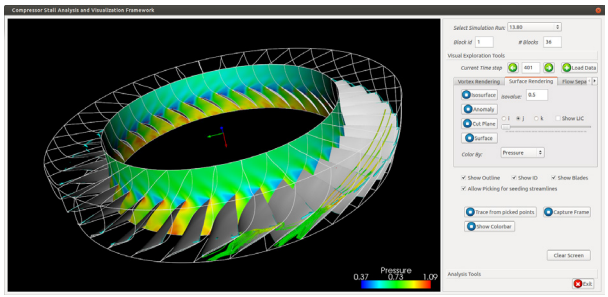

Fig. 10: The visual exploration system. The interface includes stall analysis tools and an example rendering of streamlines, isosurfaces and cut planes.

tured if we only visualize a single time step of the anomalous regions at a time. After time step 350, persistently growing anomalous regions crossing almost all passages are formed. The time step 350 found for this dataset is consistent with the drop-off of the mass flow rate shown in Figure 2a. This result suggests that anomaly analysis can be used to identify stall. Therefore, the heatmap representation achieves the goal to reveal patterns for the scientists to track the behaviors of anomalous regions for signs of possible stall cells. With this representation, the scientists can also easily find interesting time steps and passages for further stall study.

While the chart of pressure anomaly provides the expert with clues of potential stall cells and where they are located, it is desired to calculate the rotational speed of the anomalous region to further confirm a stall cell has been detected. A line widget is used to find the velocity by adjusting the end points of an event, as shown by the blue line in Figure 9. The number besides the line shows the fractional rotation speed of a stall cell to the rotor speed, where a horizontal line indicates 100% of the rotor speed. The measurement of the rotation speed reads less than 50% of the rotor speed, which, according to the expert, indicates the near-stall condition.

5.2 Integrated Visual Exploration System

After the important time steps and blade passages are identified from the visual comparison tools presented above, our visual exploration system is designed in a way that the scientists can verify the detection results and further explore the original dataset. Figure 10 shows the interface that integrates the above analysis and rendering techniques for stall analysis. The proposed system is built using VTK, which is a widely used open-source visualization library [42]. The visualization system serves two purposes required by the expert: (1) to evaluate and verify the stall analysis results, and (2) to further explore the dataset around the selected regions for enhanced understanding.

To verify that the detected passage has a tip clearance vortex angle perpendicular to the axial direction, isosurfaces of λ_2 criterion in the selected time step are used to show the orientation and size of the vortices. Since streamlines and pressure values are commonly used to affirm the existence of a vortex structure, the exploration system can display streamline traces surrounding the tip clearance vortices and cut planes of pressure values. To explore anomalous regions, the scientists look for abnormal changes of variable values including pressure, density, and entropy etc. Regions of the statistical anomalies based on the method described in Section 4.2 are rendered to provide immediate indication of abnormal regions in the selected time step. The visualization system allows the scientists to explore the data based on hypothesis formation and visual verification. In order to reach to a definitive conclusion, the system allows expert to go back and forth between the abstract plot-based visualization and data domain exploration so that they can adjust/refine their hypotheses based on visual feedbacks from the data. The proposed framework involves scientists in the exploration loop which leverages free exploration of data and knowledge discovery.

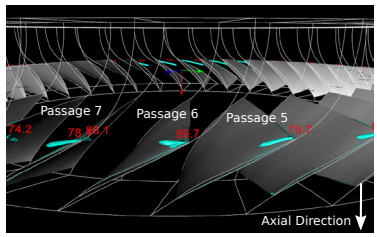

(a) Vortex regions detected by λ_2 criterion, labeled with angles to the axial direction.

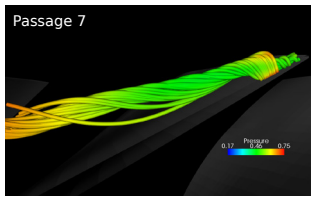

(b) Streamlines showing the tip clearance vortex of passage 7, colored in pressure.

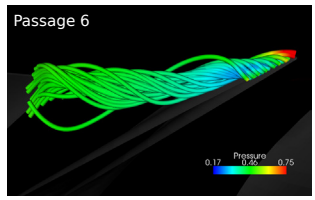

(c) Streamlines showing the tip clearance vortex of passage 6, colored in pressure.

Fig. 11: Tip clearance vortices detected at time step 361. Passage 6 shows the vortex structure more perpendicular to the axial direction.

6 Results and Expert Feedback

In this section we demonstrate the effectiveness of our visual analytics framework in a rotating stall analysis. In order to verify the two proposed stall analysis methods are able to detect stall inception, experiments in different operating conditions were performed. The analyses were then shown by our visualization interface and examined by the domain scientists. The collaboration involved an expert with more than 28 years of simulation and analysis experience on transonic turbine stages and two aerospace engineering PhD students. The expert feedback was collected from regular bi-weekly meetings in the past one and a half years, which allowed us to gradually improve the framework and the experimental design.

The compressor rotor used in experiment consists of 36 blade passages, each of which is stored in curvilinear grids of dimensions $151 \times 71 \times 56$, forming a multiblock dataset. Thus each time step requires storage of 690 MB in PLOT3D format consisting of 21.6 million grid points. The simulation divides a full turbine revolution into 3600 iterations, where the flow data is output and stored every 25 simulation iterations. In our experiments, each simulation runs at least 4 revolutions to observe whether stall occurs, which generates at least 400 GB of data with 576 time steps per dataset. Note that the time steps presented in this paper are in the unit of the stored time steps at the sampling rate of 25 simulation iterations. In the following, we first show that our visual analytics system can help detect the inception of stall, using the previously presented dataset in the stall condition. Then we demonstrate the applicability of the stall analysis system in different operating conditions to show its potential use for stall analysis and exploration. Finally, the performance measures are listed to show the efficiency of the stall analysis algorithms.

6.1 Verification of the Proposed Stall Detection Methods

In this section we will verify the proposed method for stall analysis by showing the consistency of analysis results to what the domain expert expects. The mass flow rate plot is a standard measure to stall analysis and thus the basis to verify our analysis results. For the dataset in the stall condition presented earlier, as shown in Figure 2a, the mass flow rate drops rapidly starting from around time step 350, indicating the occurrence of stall. This time step is consistent to our analysis results. Through brushing the juxtaposed charts of the tip clearance angles (Figure 8), as discussed in Section 5.1.1, we find passage 6 at time step 361 showing the vortex angle first approaching 90 degrees. Similarly, Section 5.1.2 describes that in the visualization of anomaly analysis (Figure 9), a persistent large anomalous pattern can be seen starting from around time step 350 in passages 3-6. Therefore both visual analysis tools allow scientists to detect and verify the occurrence of stall as well as pinpoint the time steps and passages where it is

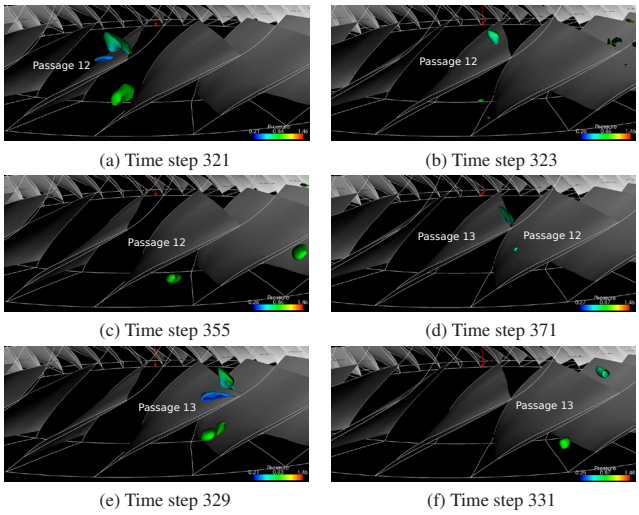

(a) Time step 321 (b) Time step 323

(c) Time step 355 (d) Time step 371

(e) Time step 329 (f) Time step 331

Fig. 12: Anomalous regions of pressure detected within time steps 321-331. These regions grow, shrink, disappear and show up again in the adjacent passage.

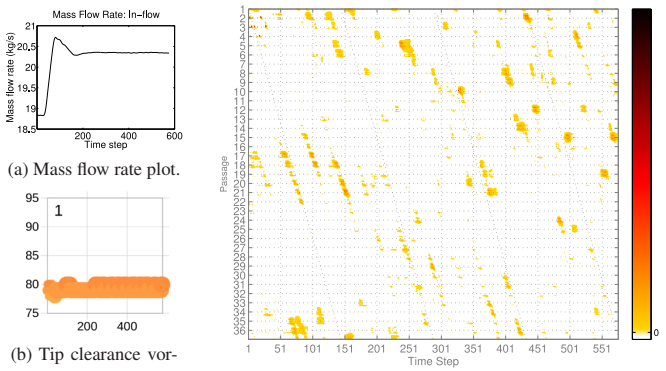

(a) Mass flow rate plot.

(b) Tip clearance vortex analysis chart.

(c) Anomaly analysis chart.

Fig. 13: Results of a stable condition using the corrected mass flow rate of 16.00 kg/s. Figure (b) shows the plot of a passage representing for all other passages in the similar behavior.

occurring. In addition to the comparison to the mass flow rate, it is necessary for the expert to inspect the raw data by visualizing the stall phenomena in the detected regions. The visual exploration system was used to examine and verify the detected regions with the expert's domain knowledge, as described in the following paragraphs.

Verification of the tip clearance vortex analysis. To inspect the structure of the tip clearance vortex found at time step 361 and verify its perpendicularity to the axial direction, our visual exploration system was used to extract isosurfaces of λ_2 measures. In Figure 11a, the isosurface representing the tip clearance vortex region in passage 6 shows a distinct vortex structure than those in other passages. The orientation also appears perpendicular to the axial direction. To observe the flow surrounding the detected vortex, Figure 11c depicts the streamlines colored by pressure value. From the vortical structure of the streamlines, it is evident that the selected region has a strong vortical flow. This demonstration shows the efficacy of the proposed juxtaposed plots to visually detect the time steps and passages having tip clearance vortex angles close to 90 degrees as a precursor of stall.

Verification of the anomaly analysis. Next, the expert was presented the heatmap visualization revealing the temporal patterns of detected anomalous regions, as previously shown in Figure 9. As discussed in Section 5.1.2, it is hypothesized that the fragmented but aligned slant patterns in the early time steps are stall cells. Since according to the expert, stall cells generally appear in areas close to blade tips, in order to verify this the system was used to render anomalous regions in selected time steps. Figure 12 shows a fixed window wherein compressor blades move to the right. The surfaces in color are the detected anomalous regions. This visualization confirms that the detected regions are close to the tip region.

Expert Feedback. By inspecting the evolution of the anomalous regions over time, an interesting phenomenon caught the attention of the domain expert. Figure 12a-b shows the anomalous regions detected in passage 12, but disappear in a later time step (Figure 12c). Later, anomalous regions are detected again in passage 13 (Figure 12d-e). This corresponds to the fragmented slant pattern seen in the anomaly analysis chart, where the fragmented pattern indicates the intermittency of the anomalies and the slant direction indicates their propagation across passages. By seeing this the expert realized that the detected anomalous regions conform to the behavior of stall cells. A brief explanation is as the following.

When stall cells occur within a passage, it forms a blockage and changes the angle of attack (AOA) of the flow. While AOA decreases in the current passage and stabilizes the flow, it increases in the neighboring passages, which in turn causes a stall there. In this way the stall cell transports from one passage to another. Therefore it is evident that the detected anomalous regions are related to stall cells.

With the evidence that the fragmented slant patterns shown in the anomaly analysis chart are stall cells, the expert hypothesized that the anomalous regions detected in the earliest time steps of this dataset are in fact stall cells. This hypothesis can be justified because the initial condition of the given dataset was already close to stall. In order to verify whether the anomaly analysis method can capture the transition from a stable to unstable condition and detect early stall inception, we ran more simulations with different throttle settings as below.

6.2 Stall Analysis of Simulations from Different Throttle Settings

In order to see the applicability of the proposed stall analysis and visualization techniques in different stability conditions, we analyzed results of simulations in different operating conditions suggested by the expert. The operating condition can be adjusted by a parameter modeling the rates of air passing through the exit throttle of the compressor in *corrected mass flow rates*. It is known that setting the corrected mass flow rate low will cause stall, while setting it high will stabilize the flow. Based on previous studies conducted on the compressor currently under investigation, stall will occur when the corrected mass flow rate is set to 13.80 kg/s, corresponding to the condition used to produce the data discussed above. To examine the capability of our stall analysis system for data generated in different conditions, we present two different throttle settings leading to different conditions: One is a known stable condition with the throttle setting 16.00 kg/s ; the other is an initially unknown condition with the setting 14.20 kg/s, which turned out to be a stall condition after a long simulation run.

6.2.1 Stable Condition (Corrected Mass Flow Rate 16.00 kg/s)

In this case the dataset was generated with a throttle setting of 16.00 kg/s from an initially less stable condition. In Figure 13a, the mass flow rate increases and stabilizes after time step 200. The visualization of the tip clearance vortices also shows no sign of stall, where the vortex angles maintain around 80 degrees. Figure 13b plots the vortex angle degrees of a passage over time, which represents all other passages in the similar stable condition.

The anomaly analysis chart in Figure 13c shows anomalous regions more scattered after time step 200. This scattered pattern is significantly different than that in the previous stall condition (Figure 9), which provides further evidence that our anomaly analysis and visualization can distinguish stable and unstable conditions.

6.2.2 Stall Condition (Corrected Mass Flow Rate 14.20 kg/s)

For this throttle setting, a corrected mass flow rate of 14.20 kg/s is used, which is in between the known stall condition (13.80 kg/s) and stable condition (16.00 kg/s). Before it turned out to be a stall condition, it was difficult to tell whether this setting would lead to stall.

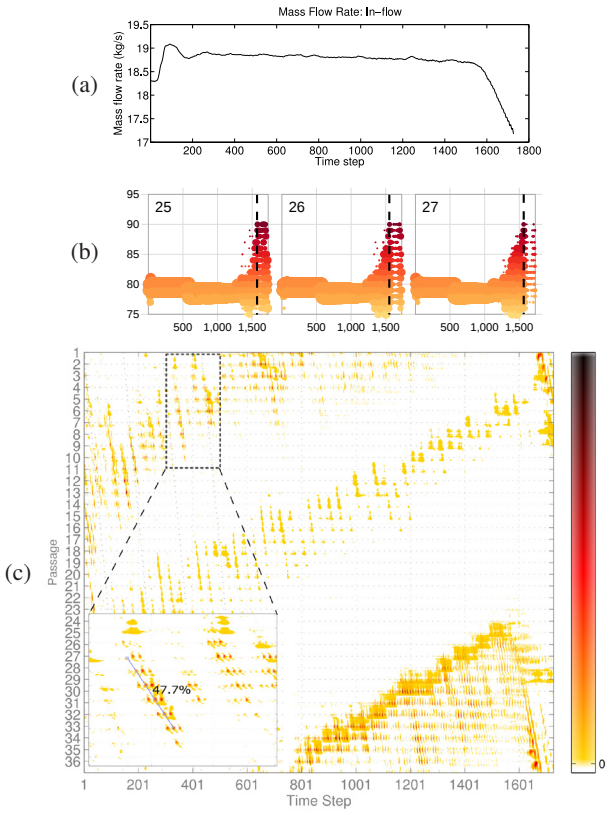

Fig. 14: Results of a stall condition using corrected mass flow rate 14.20 kg/s. (a): Mass flow rate plot. (b): Tip clearance angle analysis charts (Showing passages 25-27). (c): Anomaly analysis chart. The lower left figure shows the dashed rectangular region within passages 1-10 and time steps 300-500.

As shown in Figure 14a, the mass flow rate first increases from a less stable condition and becomes stable with small oscillations appearing after time step 300. A stable mass flow rate is maintained until approximately time step 600, where the mass flow rate begins a slow decline. Finally stall occurs at around time step 1500, or almost 10.5 rotor revolutions. The data size of the entire simulation output is 1TB.

In the tip clearance vortex analysis shown in Figure 14b, the time step when the vortex angles first become 90 degrees is also around 1500, occurring in passages 25-27. The similar time steps and passages of stall occurrence can also be observed in the anomaly analysis chart in Figure 14c. Additionally, the fragmented slant patterns continuously appear and propagate from the beginning of the simulation. These patterns are similar to that previously shown in the stall condition with the throttle setting at 13.80 kg/s (Figure 9), which correspond to the occurrence of stall cells. This experiment shows that instabilities, though not clearly picked up by mass flow rate and tip vortex analysis, are already present in earlier time steps and captured by our anomaly analysis method.

6.3 Algorithm Performance and Storage Size

To measure the performance of our stall analysis algorithms, a Linux desktop machine was used with a 7200 RPM disk, 16GB RAM and the Intel Core i7-2600 CPU supporting up to 8 concurrent threads. The algorithms were implemented with OpenMP parallelization, where the vortex angle computation was parallelized over passages and the anomaly analysis computation was parallelized over point sets. It took around two hours to complete processing a dataset of 576 time steps (four rotor revolutions). Within each time step, the computation of the λ_2 criterion on the curvilinear grids, the vortex angles and the anomaly analysis took 7.6, 0.63 and 0.42 seconds in average, respectively. The average I/O time was 1.9 seconds to load the PLOT3D files. The extracted information used for the comparative visualization, output in text formats, was less than 0.1 MB per time step. The small file size was a result of vortex analysis only storing the lengths and angles per detected vortex and the anomaly analysis only storing the count of anomalous points per angular position, as described in Section 5.1.2.

7 Discussion of the Experimental Results

The above results on various throttle settings demonstrate the capability of our visual analytics system to detect stall inception. In all tests, the identified time steps of stall are consistent with the standard mass flow rate analysis results. More importantly, the anomaly analysis and visualization, as shown in Figure 9, displays pronounced trends at a much earlier time than the other two methods (vortex angle and mass flow rate analysis). According to the expert this shows that the proposed statistics-based anomaly analysis method is able to capture instability in the flow field, and can be a useful tool to predict the ultimate occurrence of stall. Early stall detection can also avoid wasting unnecessary simulation cycles in order to determine whether a throttle setting leads to stall. This is especially useful in fine-tuning the throttle setting to find the critical stall point.

This study also demonstrates the successful application of visualization to feature detection, when the characteristics of the feature is to be discovered and the detection criteria are to be searched for. The intermittent behavior of the stall cells makes automatic detection and tracking of these stall cells difficult, since most object tracking algorithms require a certain type of spatial coherence in adjacent time frames [7, 34]. Instead, by aligning the detected regions of all time steps, our visualization of anomaly can reveal implicit patterns easy to pick up by human eyes. Since the proposed anomaly analysis approach uses a general statistics method, we believe it can be applied to stability analysis in other rotating devices as well as other data types where symmetry is present.

In terms of limitation, our current visual design does not distinguish the different locations of anomalous regions in a given passage (e.g., tip or hub area) and requires the user to visualize the original data. We plan to add more visual design elements into the heatmap, such as more colors and interaction. In addition, in order to extract tip clearance vortices, the current method requires the user input of λ_2 threshold when a new model is given. Visualization tools to aid the threshold search like predicates [39, 40] and more sophisticated extraction criteria can be applied in the future work. To obtain more precise tip clearance vortex angle, line-based vortex detection methods can be used to explicitly obtain vortex core lines. Finally, the visual exploration tool can be further improved by integrating brushing and linking techniques on 3D views and the selected tip clearance vorticies and anomalous regions from the corresponding visualizations.

8 Conclusions

We present a visual analytics system with integrated visualization techniques to help scientists study the complex phenomena of rotating stall. The system tightly couples domain knowledge into stall analysis algorithms, which efficiently extract essential information from large simulation data. The analysis results are depicted through compact and comprehensible visualization techniques using interactive plots. Our integrated visualization interface allows the scientists to verify the hypothesized stall inception regions and further explore the detected regions in detail. Experimental results and positive feedback from domain scientists provide a strong indication of the efficacy and potential of our system to help future stall analysis and precursor development. The future work is to continue the evaluation of the proposed stall analysis and visualization techniques in other operating conditions and perhaps on different compressor models.

Acknowledgments

The authors would like to thank James Giuliani for his great technical support of the TURBO simulator and constructive feedback. This work was supported in part by NSF grants IIS-1250752, program manager Almadena Chtchelkanova, IIS-1065025, and US Department of Energy grants DE-SC0007444, DE-DC0012495, program manager Lucy Nowell.

REFERENCES

[1] B. Abraham and A. Chuang. Outlier detection and time series modeling. *Technometrics*, 31(2):241–248, 1989.

[2] C. C. Aggarawal. *Outlier Analysis*. Springer New York, 2013.

[3] N. Andrienko and G. Andrienko. Coordinated views for informed spatial decision making. In *Coordinated and Multiple Views in Exploratory Visualization, 2003. Proceedings. International Conference on*, pages 44–54, 2003.

[4] R. A. Becker and W. S. Cleveland. Brushing scatterplots. *Technometrics*, 29(2):127–142, 1987.

[5] J. Bertin. *Semiology of graphics: diagrams, networks, maps*. University of Wisconsin press, 1983.

[6] A. Buja, J. A. McDonald, J. Michalak, and W. Stuetzle. Interactive data visualization using focusing and linking. In *Visualization, 1991. Visualization'91, Proceedings., IEEE Conference on*, pages 156–163. IEEE, 1991.

[7] J. Caban, A. Joshi, and P. Rheingans. Texture-based feature tracking for effective time-varying data visualization. *Visualization and Computer Graphics, IEEE Transactions on*, 13(6):1472–1479, Nov 2007.

[8] A. Y. L. Chan, J. Lee, and R. M. T. II. Visualization of vortex core differences between ensemble simulations. *IEEE Visualization Contest 2011*, 2011.

[9] V. Chandola, A. Banerjee, and V. Kumar. Anomaly detection: A survey. *ACM Comput. Surv.*, 41(3):15:1–15:58, 2009.

[10] J. Chen, R. Webster, M. Hathaway, G. Herrick, and G. Skoch. Numerical Simulation of Stall and Stall Control in Axial and Radial Compressors. In *44th AIAA Aerospace Sciences Meeting and Exhibit*. American Institute of Aeronautics and Astronautics, Jan. 2006.

[11] J.-P. Chen, M. D. Hathaway, and G. P. Herrick. Prestall Behavior of a Transonic Axial Compressor Stage via Time-Accurate Numerical Simulation. *Journal of Turbomachinery*, 130(4):041014, 2008.

[12] I. Day. Stall inception in axial flow compressors. *Journal of Turbomachinery*, 115(1):1–9, 1993.

[13] I. J. Day, T. Breuer, J. Escuret, M. AU - Cherrett, and A. AU - Wilson. Stall inception and the prospects for active control in four high-speed compressors. *Journal of Turbomachinery*, 121(1):18–27, 1999.

[14] H. Doleisch. Simvis: Interactive visual analysis of large and time-dependent 3d simulation data. In *Simulation Conference, 2007 Winter*, pages 712–720, 2007.

[15] D. Ericson, J. Johansson, and M. Cooper. Visual data analysis using tracked statistical measures within parallel coordinate representations. In *Coordinated and Multiple Views in Exploratory Visualization, 2005. (CMV 2005). Proceedings. Third International Conference on*, pages 42–53, 2005.

[16] E. Eskin. Anomaly detection over noisy data using learned probability distributions. In *the Seventeenth International Conference on Machine Learning*, pages 255–262, 2000.

[17] M. Gleicher, D. Albers, R. Walker, I. Jusufi, C. D. Hansen, and J. C. Roberts. Visual Comparison for Information Visualization. *Information Visualization*, 10(4):289–309, 2011.

[18] N. Görnitz, M. Kloft, K. Rieck, and U. Brefeld. Toward supervised anomaly detection. *J. Artif. Int. Res.*, 46(1):235–262, 2013.

[19] D. Gresh, B. Rogowitz, R. Winslow, D. Scollan, and C. Yung. Weave: a system for visually linking 3-d and statistical visualizations applied to cardiac simulation and measurement data. In *Visualization 2000. Proceedings*, pages 489–492, 2000.

[20] F. E. Grubbs. Sample criteria for testing outlying observations. *The Annals of Mathematical Statistics*, pages 27–58, 1950.

[21] M. Hathaway, G. Herrick, J. Chen, and R. Webster. Time accurate unsteady simulation of the stall inception process in the compression system of a US army helicopter gas turbine engine. In *Computer Architecture, 2004. Proceedings. 31st Annual International Symposium on*, pages 166–177, 2004.

[22] V. Hodge and J. Austin. A survey of outlier detection methodologies. *Artif. Intell. Rev.*, 22(2):85–126, 2004.

[23] D. A. Hoying, C. S. Tan, H. D. Vo, and E. M. Greitzer. Role of Blade Passage Flow Structures in Axial Compressor Rotating Stall Inception. *Journal of Turbomachinery*, 121:735–742, 1999.

[24] J. Hunt. Vorticity and vortex dynamics in complex turbulent flows. *Canadian Soc. for Mechanical Eng., Trans.*, 11(1):21–35, 1987.

[25] J. Jeong and F. Hussain. On the identification of a vortex. *Journal of Fluid Mechanics*, 285:69–94, 1995.

[26] M. Jiang, R. Machiraju, and D. S. Thompson. Detection and visualization of vortices. In *Visualization Handbook*, pages 287–301. Academic Press, 2004.

[27] J. Kehrer, H. Piringer, W. Berger, and M. E. Groller. A model for structure-based comparison of many categories in small-multiple displays. *Visualization and Computer Graphics, IEEE Transactions on*, 19(12):2287–2296, 2013.

[28] E. M. Knox and R. T. Ng. Algorithms for Mining Datasets Outliers in Large Datasets. *24th International Conference on Very Large Data Bases*, pages 392–403, 1998.

[29] B. Kohler, R. Gasteiger, U. Preim, H. Theisel, M. Gutberlet, and B. Preim. Semi-Automatic Vortex Extraction in 4D PC-MRI Cardiac Blood Flow Data using Line Predicates. *Visualization and Computer Graphics, IEEE Transactions on*, 19(12):2773–2782, Dec. 2013.

[30] X. Liu, Y. Hu, S. North, and H.-W. Shen. Correlatedmultiples: Spatially coherent small multiples with constrained multi-dimensional scaling. *Computer Graphics Forum*, 2015.

[31] X. Liu and H.-W. Shen. The effects of representation and juxtaposition on graphical perception of matrix visualization. In *Proceedings of the 33rd annual ACM conference on Human factors in computing systems*. ACM, 2015.

[32] S. Ljevar, H. C. de Lange, and a. a. van Steenhoven. Two-dimensional rotating stall analysis in a wide vaneless diffuser. *International Journal of Rotating Machinery*, 2006:1–11, 2006.

[33] N. M. McDougall, N. A. Cumpsty, and T. P. Hynes. Stall inception in axial compressors. *Journal of Turbomachinery*, 112(1):116–123, 1990.

[34] F. H. Post, B. Vrolijk, H. Hauser, R. S. Laramee, and H. Doleisch. The State of the Art in Flow Visualisation: Feature Extraction and Tracking. *Computer Graphics Forum*, 22(4):775–792, 2003.

[35] S. Ramaswamy, R. Rastogi, and K. Shim. Efficient algorithms for mining outliers from large data sets. *Proceedings of the 2000 ACM SIGMOD international conference on Management of data - SIGMOD '00*, 29:427–438, 2000.

[36] L. Reid and R. Moore. Performance of single-stage axial-flow transonic compressor with rotor and stator aspect ratios of 1.19 and 1.26, respectively, and with design pressure ration of 1.82. *NASA Technical Paper*, 1978.

[37] J. Roberts. State of the art: Coordinated multiple views in exploratory visualization. In *Coordinated and Multiple Views in Exploratory Visualization, 2007. CMV '07. Fifth International Conference on*, pages 61–71, 2007.

[38] F. Sadlo, R. Peikert, and E. Parkinson. Vorticity based flow analysis and visualization for pelton turbine design optimization. In *IEEE Visualization, 2004.*, pages 179–186, 2004.

[39] T. Salzbrunn, C. Garth, G. Scheuermann, and J. Meyer. Pathline predicates and unsteady flow structures. *The Visual Computer*, 24(12):1039–1051, 2008.

[40] T. Salzbrunn and G. Scheuermann. Streamline predicates. *IEEE Transactions on Visualization and Computer Graphics*, 12(6):1601–1612, 2006.

[41] T. Schafhitzel, J. E. Vollrath, J. P. Gois, D. Weiskopf, A. Castelo, and T. Ertl. Topology-Preserving $\lambda 2$-based Vortex Core Line Detection for Flow Visualization. *Computer Graphics Forum*, 27(3):1023–1030, 2008.

[42] W. Schroeder, K. Martin, and B. Lorensen. The Visualization Toolkit. *Kitware*, 2006.

[43] S. Shafii, H. Obermaier, R. Linn, E. Koo, M. Hlawitschka, C. Garth, B. Hamann, and K. I. Joy. Visualization and analysis of vortex-turbine intersections in wind farms. *IEEE transactions on visualization and computer graphics*, 19(9):1579–91, Sept. 2013.

[44] S. Stegmaier, U. Rist, and T. Ertl. Opening the Can of Worms: An Exploration Tool for Vortical Flows. In *IEEE Visualization 2005*, pages 463–470. IEEE Computer Society, 2005.

[45] J. K. Taylor and C. Cihon. *Statistical Techniques for Data Analysis*. Chapman and Hall/CRC, 2nd edition, 2004.

[46] E. R. Tufte. *Envisioning Information*. Graphics Press, 1990.

[47] C. Turkay, A. Slingsby, H. Hauser, J. Wood, and J. Dykes. Attribute signatures: Dynamic visual summaries for analyzing multivariate geographical data. *Visualization and Computer Graphics, IEEE Transactions on*, 20(12):2033–2042, Dec 2014.

[48] H. D. Vo, C. S. Tan, and E. M. Greitzer. Criteria for Spike Initiated Rotating Stall. *Journal of Turbomachinery*, 130(1):011023, 2008.

[49] J. N. Wilson and G. X. Ritter. Connected Component Algorithms. In *Handbook of Computer Vision Algorithms in Image Algebra*, chapter 6, pages 173–185. CRC Press, 2nd edition, 2000.